Cement and Concrete Research 41 (2011) 403–411

Contents lists available at ScienceDirect

Cement and Concrete Research

journal homepage: http://ees.elsevier.com/CEMCON/default.asp

Modelling of ageing effects on crack-bridging behaviour of AR-glass multifilament yarns embedded in cement-based matrix

M. Butler, S. Hempel, V. Mechtcherine *

Institute of Construction Materials, TU Dresden, Dresden, Germany

ARTICLE INFO

Article history:
Received 22 October 2009
Accepted 12 January 2011

Keywords:
SEM (B)
Aging (C)
Micromechanics (C)
Fiber Reinforcement (E)
Modeling (E)

ABSTRACT

This article focus on modelling of ageing effects on crack-bridging behaviour of AR-glass multifilament yarns embedded in cement-based matrix. In the first step, age-dependent changes in the crack-bridging behaviour of AR-glass multifilament yarns were investigated at the meso and micro levels. Two cementitious matrices were considered where the binder contained Portland cement clinker and ground granulated blast furnace slag cement, respectively. Mechanical characteristics of the bond between matrix and multifilament yarns after accelerated ageing were measured by means of double-sided yarn pullout tests. In these tests the multifilament yarns bridged a single crack in the matrix arising in a notched area of the specimen. Losses in performance with increasing age differed widely depending on matrix material composition. The essential cause of such losses was discovered to be the microscopic densification of the fibre-to-matrix interface. This led to increased bond intensity and restricted slip-ability of the filaments. Subsequently, these micro-structural phenomena were related to the mesoscopic material behaviour by means of a phenomenological bond model. This cross-linkage model describes the crack-bridging effect of the entire multifilament yarn at the single filament level. According to the model, each filament possesses a specific deformation length depending on its position in the cross-section of the yarn. This deformation length depends on bond characteristics between single filament and cementitious matrix, which vary with age. Characteristic values of the model were computed from load-crack width curves obtained from the yarn pullout tests. The changes in the microstructure were represented by the characteristic values of the model.

1. Introduction

Textile-reinforced concrete (TRC) is a composite construction material consisting of high performance, multifilament yarns of glass or carbon fibre and a matrix of fine-grained concrete. In existing applications of TRC, chiefly fabrics made of alkali resistant glass fibres (so-called AR glass) are used. The main features of TRC are its toughness, high tensile strength and pronounced ductile behaviour. TRC can be applied both in the fabrication of new structures and in the strengthening and repair of structural elements made of reinforced concrete or other traditional materials as well [1].

Most of these applications require that the high tensile strength and toughness of TRC do not degrade significantly with increasing age. Changes in the mechanical performance of the composite can result from deterioration of the reinforcing AR-glass fibres themselves due to the attack of OH^--ions in the pore solution (e.g. [2–4]), the static fatigue (delayed failure) of the glass fibre under sustained load in the highly alkaline environment (e.g. [5–8]), and changes in the bond between matrix and fibres (e.g. [9–12]). The last-mentioned effect results mainly from the densification of the matrix adjacent to the filaments and the intensified fibre–matrix bond with continued hydration. Furthermore, accumulation of hydration products at the interface between filaments and matrix and in the empty spaces between the filaments of multifilament yarn (bundle filling) can precipitate these changes in the mechanical performance.

In this paper the contribution of individual damage mechanisms to degradation of crack-bridging behaviour of multifilament yarn and their interaction is shown by means of a simple phenomenological model. The model is based on experimental data obtained from multifilament yarn pullout testing and micro-structural investigation of the yarn–matrix interface [14–16]. Some of this data is briefly presented in the experimental part of this article.

2. Experiments

2.1. Test method – double-sided yarn pullout

The crack-bridging performance of multifilament yarn was evaluated using double-side pullout testing. In these pullout tests various artefacts resulting from a complex geometry of technical textiles are excluded, thus allowing a straightforward interpretation of the results obtained. Doubly symmetrical, bone shaped prisms

---

* Corresponding author. Tel.: +49 351 463 35 920.
E-mail address: MECHTCHERINE@tu-dresden.de (V. Mechtcherine).

0008-8846/$ – see front matter © 2011 Elsevier Ltd. All rights reserved.
doi:10.1016/j.cemconres.2011.01.007

featuring a notch of depth 1 mm in the middle were used as specimens (Fig. 1).

Each specimen was reinforced with three parallel oriented multifilament yarns extending over the entire length of the specimen. The amount of reinforcement was chosen in such way that multiple cracking was avoided and only a single-crack formed at the notch.

During casting the reinforcing yarns were fixed on a stretching frame in order to embed them tautly into the fine-grained concrete. The specimens were demoulded one day after fabrication. At this time the three imbedded reinforcing yarns were detached from the stretching frame.

After demoulding all specimens were stored for 6 days in water (20 °C). Subsequently, a small number of specimens were subjected to reference storage (20 °C/65% RH) until testing at an age of 28 days. The remaining test specimens were subjected to accelerated ageing in a fog room (40 °C/99% RH). The periods of fog room storage were 28, 56, 90, 180 and 360 days.

The pullout testing was performed under controlled deformation conditions defined by a crack opening rate of 1 mm/min.

2.2. Materials – yarn and fine-grained concrete

Multifilament yarn made of AR-glass (type CEMFIL) was used as reinforcing material in the pullout tests. The multifilament yarn consists of 1600 individual filaments with a mean diameter of 13.6 μm. The mean tensile strength of such filaments is 1917 MPa and their mean strain capacity 0.0258.

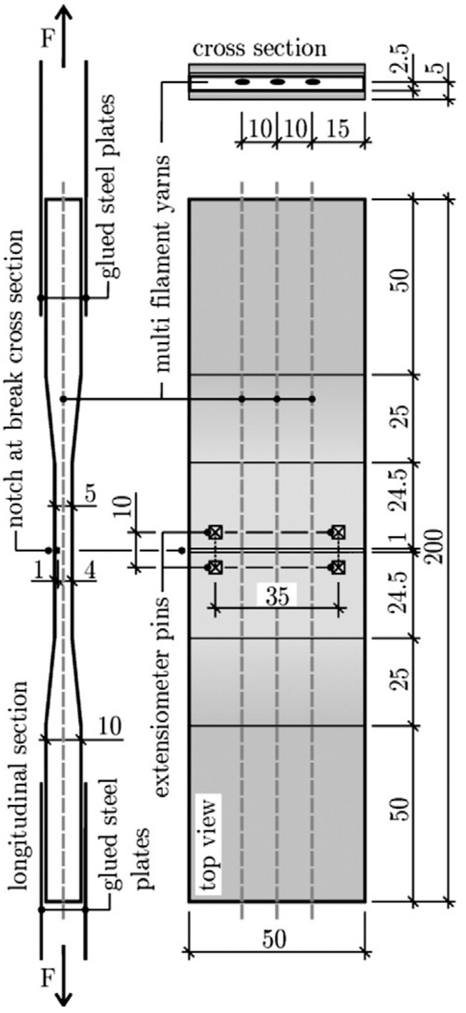

Fig. 1. Specimen geometry for pullout test, arrangement of yarn reinforcement (geometrical data in mm).

Two fine-grained concrete mixtures (M1, M2, cf. Table 1) were used as matrix materials. The maximum grain size of the matrices is 1 mm. The matrices differ in binder composition and therefore in alkalinity, hydration kinetics and binder granulometry.

In matrix M1 the appearance of $Ca(OH)_2$ (abbrev.: C-H) and alkalis is substantially reduced due to the high content of ground granulated blast furnace slag (ggbs) in the cement and the presence of fly ash and micro-silica in the binder. The pH decreases from an initial value of 12.4 to approximately 11.8 after 360 days of ageing. Matrix M2 shows a less pronounced diminution of pH from 12.6 to 12.4, caused by the absence of ggbs and therefore higher Portland cement clinker content in cement. The pH measurement was performed on filtered slurry of dry ground matrix material, taken from inner parts of concrete prisms, using a calibrated digital pH-meter.

The qualitative alteration of CH content in the hardened matrix was evaluated by ESEM investigation. Since the microscopic study was limited to the observation of the morphology of hydration products, no quantitative results on the hydration phases could be obtained. Also no chemical analysis of individual phases was performed. However, for the purpose of this study, i.e. to provide the background for a micromechanically based model, it was sufficient to distinguish qualitatively between the main phases Calcium–Silicate–Hydrates (abbrev. C–S–H), ettringite and $Ca(OH)_2$. Truly, it is not known, if and how the presence of glass fibre influences the chemistry of the hydration products. This is still to be investigated. The working hypothesis of this study was that possible effect of glass fibre on hydration products can be neglected. The main interest was to investigate the trend of the formation of the hydration products in the interphase between fibres and matrix for two matrices with different binder composition. Qualitative descriptions like "higher CH content" or "denser microstructure" were used.

For the ESEM investigation the specimens (cf. Fig. 1) were segmented and eventually splitted along the embedded multi-filament yarns. To prove whether this preparation technique influenced the morphology of the interphase between filaments and matrix some samples were prepared not by splitting but by resin impregnation and sawing of TRC specimens with subsequent polishing of the surface and gold sputtering prior to the ESEM investigation.

3. Results

3.1. Double-sided pullout tests

The characteristic pullout curves of specimens with geometry according to Fig. 1 are shown in Figs. 3 and 5. Each curve depicted represents a best-fit curve based on at least 7 individual pullout curves. The fit was made by smoothing the average curve of the individual curves.

The pullout curves are presented in simplified form (Fig. 2). The curves measured in the experiments can be divided in three parts: zone I – the macroscopic un-cracked state of specimen, zone II – a snap-back branch due to under-critical reinforcement of specimen and zone III – the pullout curve being of interest. In the diagrams

Table 1
Composition of matrices M1 and M2 [kg/m³].

Matrix constituent	M1	M2
CEM I 32,5 R	–	557
CEM III/B 32.5 NW-HS-NA	550	–
Fly ash	248	251
Microsilica[a]	55	56
Sand 0/1 mm	1101	1114
Water	248	251

[a] Suspension; 50 M.% powder, 50 M.% water.

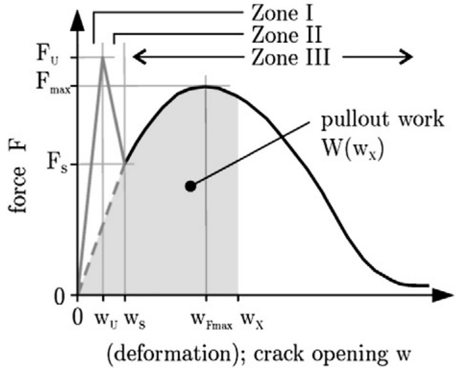

Fig. 2. Schematic representation of typical pullout curve, indication of characteristic values.

below, the curve branches describing zone I and zone II are neglected and replaced by an interpolated line from $F(w=0)=0$ to the point where the yarn pullout is initiated (dashed line in Fig. 2). The pullout works were determined by integration of areas below the pullout curve as indicated in Fig. 2.

Fig. 3 displays the characteristic pullout curves of matrix M1 samples. The mechanical performance of the bond decreases with increasing duration of accelerated ageing. The maximum fibre pullout force F_{max} decreases by approximately 25% after 360 days of accelerated ageing, whilst the pullout work during crack opening decreases by approximately 40% compared to the reference specimens (see F_{max}, $W_{0.25}$ and $W_{0.5}$ in Fig. 4).

In Fig. 5 the pullout curves of matrix M2 specimens are shown. The maximum yarn pullout force F_{max} of the reference specimens is approximately 10% higher in comparison to the tests on matrix M1 samples (cf. Fig. 3). The pullout work of the matrix M2 reference specimens is similar to the corresponding values for the matrix M1 reference specimens. With increasing age of the matrix M2 samples, the tendency to decrease the maximum pullout force F_{max} as well as pullout energy is more distinct than for matrix M1 specimens (cf. Figs. 4 and 6).

3.2. Microstructural investigations

Fig. 7 represents the characteristic microstructure in the interface between the multifilament yarn's sleeve filaments and matrix M1 after 28 days' reference storage. The single filaments are embedded in an inhomogeneous matrix consisting of un-hydrated binder particles and hydration products as Calcium–Silicate–Hydrates ettringite and $Ca(OH)_2$. The matrix shows a structure which is not yet very dense. Contact between the hydration products and the filament surface is visible only at discrete points. In Fig. 7a the state of fibre–matrix interphase as observed after splitting a specimen, i.e. a fracture surface is shown. Fig. 7b displays the interphase after sawing, polishing and gold sputtering. Both methods provide similar results with regard to the quality of micrographs.

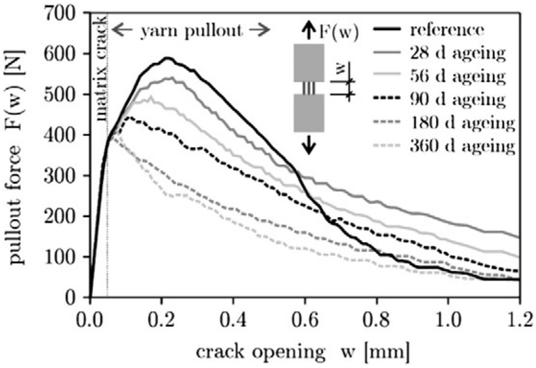

Fig. 3. Force vs. crack opening curves of matrix M1 specimens; storage at 40 °C/99% RH, reference at 20 °C/65% RH.

In Fig. 8 the morphology of the M1 fibre–matrix-combination after 360 days' accelerated ageing is illustrated. Due to the ongoing hydration process the matrix becomes denser in comparison to Fig. 7. In Fig. 8a (fracture surface) this is better recognisable than in Fig. 8b (polished surface). The single filaments are embedded in hydration products composed as described in the paragraph above. But here the C–S–H phases are considerably more abundant near the single filaments and the matrix seems to be more densified due to the increased content of C–S–H phases which can be identified by their slender, tightly interlocked morphology. Therefore, the filaments are encased mostly by these delicate C–S–H phases on large surface areas which form nearly homogeneous encasements and assure a good bond performance in the interphase.

The micrographs confirm the fact of a slowly continuing hydration process for binder compositions with a low Portland cement clinker content, ground granulated blast furnace slag and pozzolana (cf. composition of M1 in Table 1). The pozzolanic reactions lead to a consumption of CH accompanied by an increase in the C–S–H content.

Fig. 9 shows filaments bonded to matrix M2 after 360 days of accelerated ageing. The filaments are covered by mineral deposits mainly consisting of C–S–H phases. Due to the usage of CEM I cement (cf. Table 1), the morphological structure of hydration products as shown in Fig. 9 is denser in comparison to Fig. 8 and it encloses the filament surfaces to a larger extend. The transition zone adjacent to filaments surface becomes stronger and stiffer with rising content of C–S–H with increasing age in comparison to the composite made with the matrix M1. However, these increases in the strength and stiffness are not necessary beneficial with regard to the composite performance in terms of its strength and ductility, cf. Figs. 3 and 5. A more detailed discussion will follow in Section 4.

4. Adhesive cross-linkage model

4.1. Phenomenological basics of model

As shown in Section 3.2, the bond between filament and cementitious matrix is non-uniform. The hydration products form adhesive cross-links between matrix and filament or filament and filament, respectively (cf. Fig. 7). The bond properties of the cross-links depend on the characteristics of hydration products, which are influenced by the binder composition, the filament-sizing, and the condition and duration of hydration (e.g. [14]). However, the cross-links reduce or prevent the displacement of the filaments (e.g. [12]).

The basic idea of the adhesive cross-linkage model was proposed by Schorn [13] and is based on the assumption that between two cross-links the filament can be deformed along the so-called available deformation length L_0. In Fig. 10 different types of bonding between filament and matrix and therefore different available deformation lengths are shown.

Due to the shear stiffness of adhesive cross-links and the linkage between filaments, an effective deformation length L_W is educed exceeding the available deformation length L_0 of the filament (cf. Fig. 10d). In the following the term “deformation length” is used synonymously with “effective deformation length”.

4.2. Distribution of deformation lengths

Because of the tiny distances between the filaments, the relatively large binder particles cannot penetrate into the inner part of the multifilament yarn. Only hydration products can reach the yarn's core. For this reason the frequency of cross-links decrease significantly from the sleeve filaments to the inner filaments.

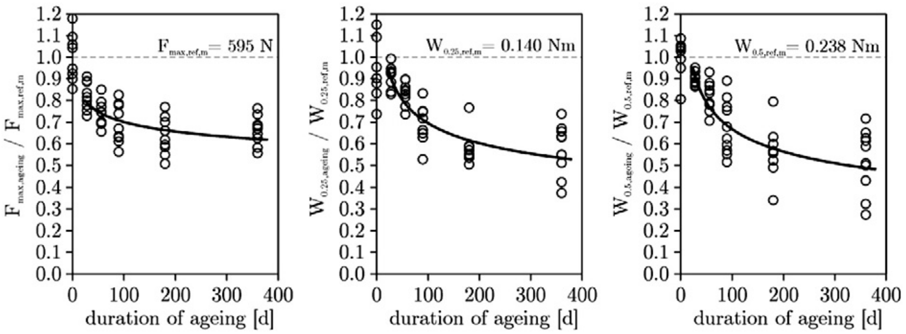

Fig. 4. Maximum pullout force F_{max} and pullout work $W_{0.25}$ and $W_{0.5}$ at the crack opening of 0.25 mm and 0.5 mm, respectively, vs. duration of ageing (matrix M1).

According to the cross-link model each filament has a specific deformation length depending on its position in the cross section of the yarn. In Fig. 11a a possible arrangement of deformation lengths over yarn diameter is sketched.

To model the crack-bridging behaviour of multifilament yarn, the indication of the deformation lengths of all filaments in the yarn becomes necessary. Fig. 11b illustrates a possible distribution of deformation lengths L_W. In this view the individual filament n is sorted according to its deformation length independent of its position in the yarn. The short deformation lengths of sleeve filaments are concentrated on top of the y-axis, the large deformation lengths of core filaments on the bottom.

4.3. Modelling the yarn's crack-bridging behaviour

The deformation length of the filament determines the crack width at which the ultimate filament strain is reached. The filament stress at defined crack openings can be calculated according to Eq. (1):

$$\sigma_n = E_n \varepsilon_n = E_n \frac{w}{L_{Wn}} \tag{1}$$

where σ = stress; E = Young's modulus; L_W = deformation length of the filament, and w = crack width.

With increasing crack width w, the filaments fail sequentially when each individual filament's strength is exceeded according to its deformation length. The load born by the failed filament is released to all other, still surviving filaments. According to Eq. (1), the stress level σ in a filament increases with decreasing L_W-value for a given crack-opening. Furthermore, cross-links can fail if their shear strength is exceeded before the maximum filament stress is reached. In this case, the associated deformation length increases. The crack-bridging load transferred by the entire multifilament yarn across the crack at crack width w can be determined according to Eq. (2):

$$F = \sum_{n=1}^{N-n_f} F_n = \sum_{n=1}^{N-n_f} \sigma_n A_n = \sum_{n=1}^{N-n_f} A_n E_n \frac{w}{L_{Wn}} \tag{2}$$

where F = crack-bridging force; A = cross section of filament; N = total number of filaments; and n_f = number of failed filaments.

In Fig. 12 the distribution of deformation lengths is indicated for a parabolic arrangement of deformation lengths around yarn diameter in a yarn with circular cross-section. At the yarn's core 10% of filaments are assumed inactive in crack-bridging load transfer; also cross-link failure is excluded. The resulting filament stresses, the crack-bridging load, and the number of failed filaments are indicated for crack width for both $w = 0.1w_{max}$ and $w = 0.5w_{max}$, respectively. At the crack width of $w = 0.1\ w_{max}$ all filaments are still un-cracked. The filament featuring the shortest deformation length L_w just reached its failure strain and its strength, respectively (at the peak of the dashed line). Up to this point the pullout crack width curve is linear. After widening the crack up to $w = 0.5\ w_{max}$, approximately the half part of all filaments failed after reaching its failure strain (represented by the hatched area). Due to the sequential failure of filaments during crack opening the pullout crack width curve becomes non-linear. The maximum pullout load was reached after failing of approximately 1/3 of all filaments.

4.4. Recursive determination of distribution of deformation lengths

The adhesive cross-linkage model enables a specific correlation between the bonding situation of a multifilament yarn embedded in cementitious matrix and its mechanical behaviour when bridging a single crack. For computation of a load-crack width curve, knowledge of the distribution of the filaments' deformation lengths is indispensable. But the experimental determination of position, strength, and stiffness of cross-links between matrix and filament as well as between filaments is nearly impossible. The cross-links haven't an exact physical counterpart; they are rather an idealised abstraction of several bonding phenomena (cf. Section 3.1).

However, the distribution of deformation lengths can be computed based on experimental data observed in pullout tests (cf. Section 2.1). In the initial phase of the recursive calculation process, it is assumed that all filaments have failed at crack width $w_{max} = w_U$, including the filaments possessing the maximum deformation length $L_{W,max}$. Hence, the number of intact filaments $M_U = 0$. At this point no further load is transmitted over the crack: $F_U = 0$. This initial state is summarised in Eq. (3), where $L_{W,V}$ is the deformation length at each iteration of recursive calculation of deformation length:

$$w = w_{max} = w_U;\ F_U = M_U = 0\ ;\ L_W = L_{W,\,max} = L_{W,V} \tag{3}$$

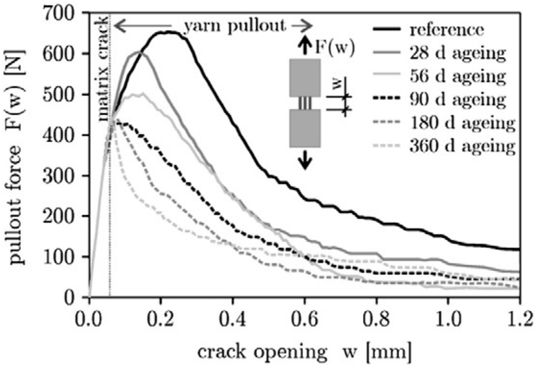

Fig. 5. Force vs. crack opening curves of matrix M2 specimens; storage at 40 °C/99% RH, reference at 20 °C/65% RH.

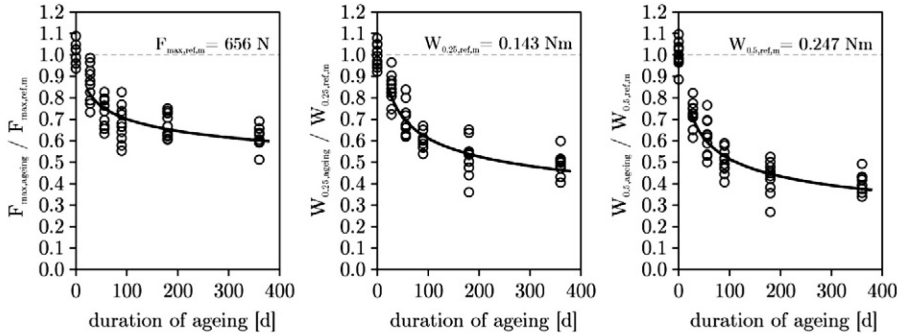

Fig. 6. Maximum pullout force F_{max} and pullout work $W_{0.25}$ and $W_{0.5}$ at the crack opening of 0.25 mm and 0.5 mm, respectively, vs. duration of ageing (matrix M2).

Before the state according to Eq. (3) is reached, at crack with w_{U-1} a load F_{U-1} is transferred via a number of uncracked filaments. The number of these uncracked filaments is given by M_{U-1}. The deformation length of these filaments is $L_{W,V-1}$, where $L_{W,V-1}<L_{W,V}$. $L_{W,V}$ represents the maximum deformation length (cf. Eq. (3)) If Young's Modulus E and the cross section A of the load bearing filaments are known, their total number M_{U-1} can be calculated according Eqs. (4) and (5):

$$w = w_{U-1} : F_{U-1} = E_F A_F \frac{w_{U-1}}{L_{W,V-1}} m_{U-1} \tag{4}$$

$$\rightarrow m_{U-1} = M_{U-1} = \frac{F_{U-1}}{E_F A_F w_{U-1}} \; L_{W,V-1} \tag{5}$$

Reducing the crack width by a further decrement at w_{U-2}, the crack-bridging load is F_{U-2}. The load is composed of two parts. One part results from the load bearing by filaments, which will fail not before the crack width w_{U-1} is reached (cf. Eq. (4)). The other part of load is provided by the filaments which will fail just at the actual crack width w_{U-2}. Accordingly, the total number of intact filaments M_{U-2} is composed of the number of filaments m_{U-1} (which stay uncracked

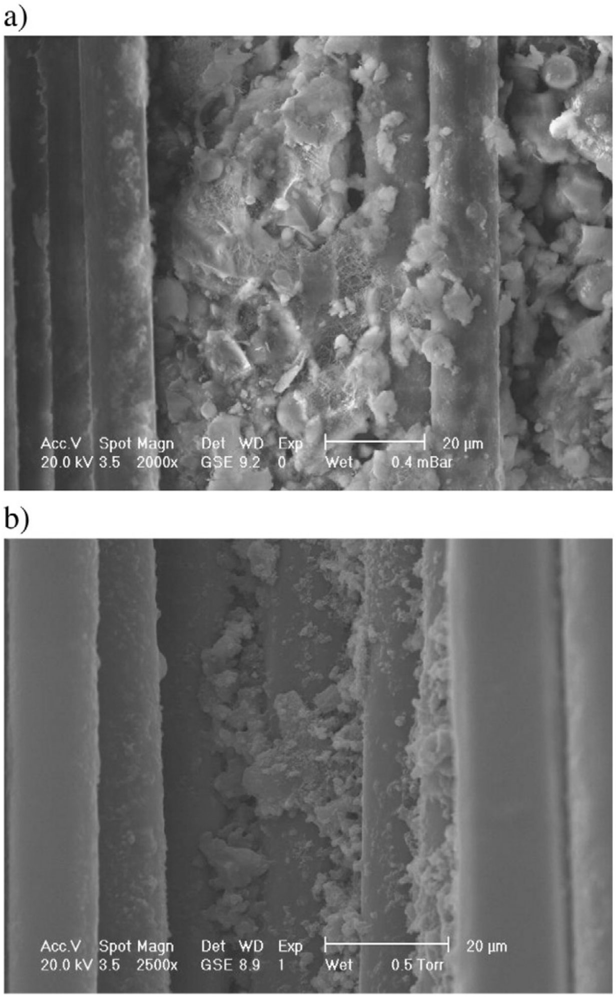

Fig. 7. ESEM image of AR glass filaments in matrix M1, 28 days of reference storage (20 °C/65% RH) a) Fracture surface, b) Polished section; gold sputtered.

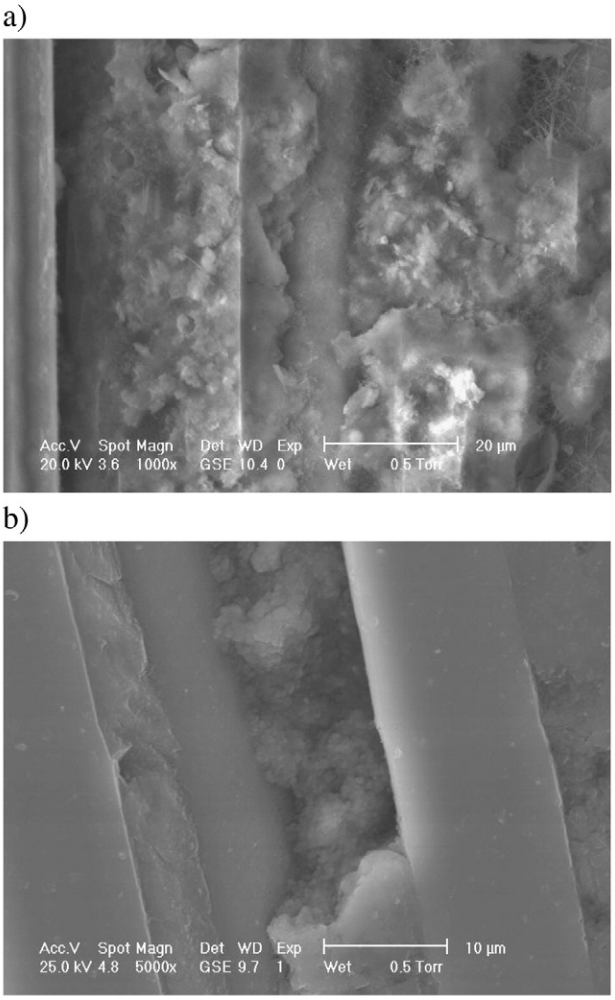

Fig. 8. ESEM image of AR glass filaments in matrix M1, 360 days of accelerated ageing (40 °C/99% RH) a) Fracture surface, b) Polished section; gold sputtered.

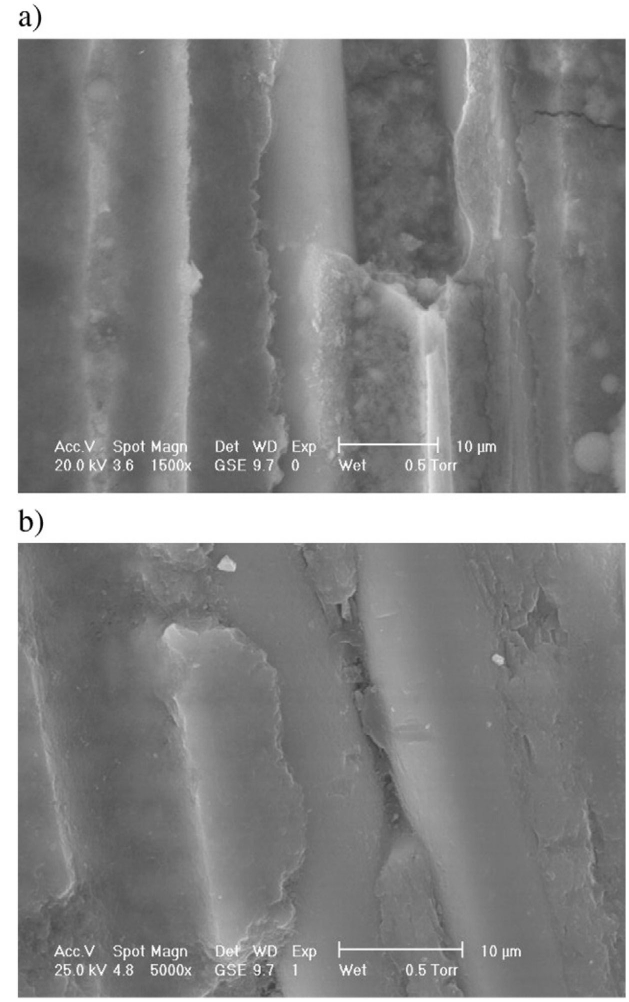

Fig. 9. ESEM image of AR glass filaments in matrix M2, 360 days of accelerated ageing (40 °C/99% RH) a) Fracture surface, b) Polished section; gold sputtered.

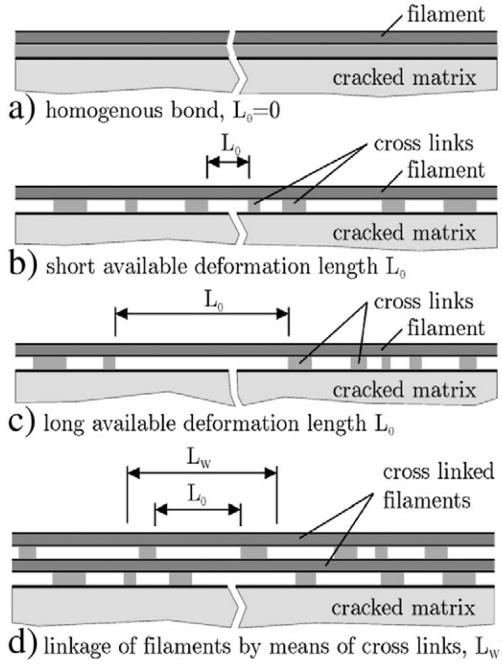

Fig. 10. Different types of bonding produce different available deformation lengths of filaments.

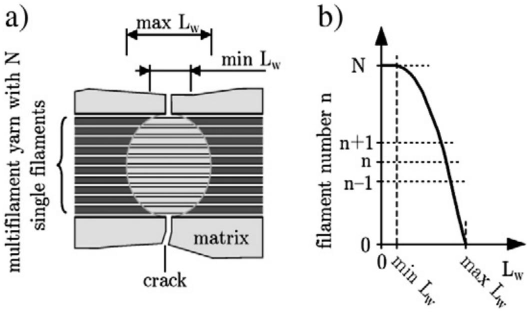

Fig. 11. a) Arrangement of deformation lengths over diameter of yarn and b) their distribution over filament number.

until crack width w_{U-1}) and the number of filaments m_{U-2} which fail during crack opening from w_{U-2} to w_{U-1} (cf. Fig. 13). However, the total crack bridging load F_{U-2} results from the particular straining of both filament groups, m_{U-1} and m_{U-2}, respectively; see Eq. (6). Considering the results of Eq. (5), m_{U-2} can now be calculated according Eq. (7):

$$w = w_{U-2} : F_{U-2} = E_F A_F \left(\frac{w_{U-2}}{L_{W,V-1}} m_{U-1} + \frac{w_{U-2}}{L_{W,V-2}} m_{U-2} \right) \tag{6}$$

$$\rightarrow m_{U-2} = \left(\frac{F_{U-2}}{E_F A_F w_{U-2}} - \frac{m_{U-1}}{L_{W,V-1}} \right) L_{W,V-2} \tag{7}$$

$$M_{U-2} = m_{U-1} + m_{U-2} \tag{8}$$

At any crack width w_{U-i}, where ($U>i>1$), the crack-bridging load F_{U-i} is composed of i individual load components, resulting from m strained filaments inside each filament group (Eq. (12), Fig. 13). The number of filaments m_{U-i} failing during crack opening from w_{U-i} to

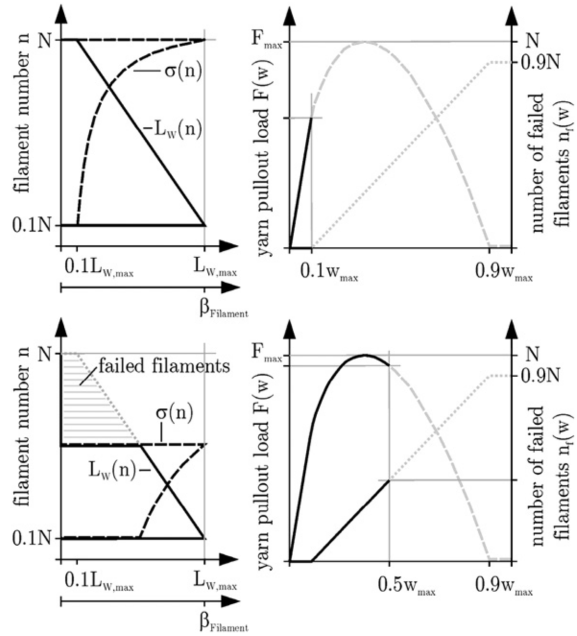

Fig. 12. Deformation lengths of filaments L_W, filament stress σ, yarn pullout load F and number of failed filaments n_f for crack width $w=0.1w_{max}$ (top) and $w=0.5w_{max}$ (bottom).

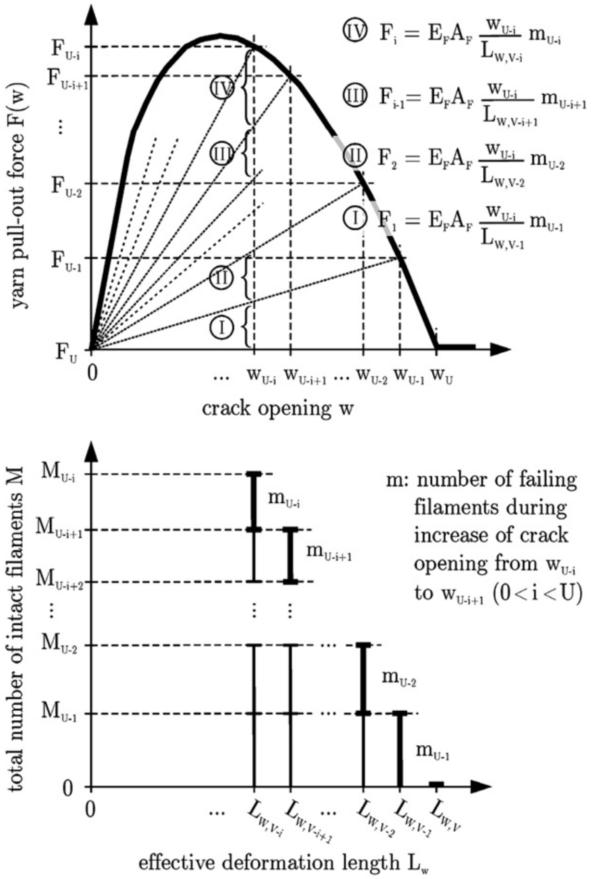

Fig. 13. Sketch of calculation process of recursive determination of distribution of filament's deformation lengths based on measured pullout load-crack width curve.

w_{U-i+1} can be calculated according to Eq. (10) and the total number of intact filaments M_{U-i} using the corresponding Eq. (11):

$$w = w_{U-i} : F_{U-i} = E_F A_F \left(\frac{w_{U-i}}{L_{W,V-1}} m_{U-1} + \frac{w_{U-i}}{L_{W,V-2}} m_{U-2} + \cdots\cdots + \frac{w_{U-i}}{L_{W,V-i+1}} m_{U-i+1} + \frac{w_{U-i}}{L_{W,V-i}} m_{U-i} \right) \tag{9}$$

$$\rightarrow m_{U-i} = \left(\frac{F_{U-i}}{E_F A_F w_{U-i}} - \left[\frac{m_{U-1}}{L_{W,V-1}} + \frac{m_{U-2}}{L_{W,V-2}} + \cdots \cdots + \frac{m_{U-i+1}}{L_{W,V-i+1}} \right] \right) L_{W,V-i} = \left(\frac{F_{U-i}}{E_F A_F w_{U-i}} - \sum_{k=1}^{i-1} \frac{m_{U-k}}{L_{W,V-k}} \right) L_{W,V-i} \tag{10}$$

$$M_{U-i} = m_{U-1} + m_{U-2} + \cdots + m_{U-i+1} + m_{U-i} = \sum_{k=1}^{i} m_{U-k} \tag{11}$$

To calculate the number of filaments m_{U-i} the specification of the deformation length of filaments $L_{W,V-i}$ is indispensable. This definition is based on the failure strain of filaments as shown in Eq. (12):

$$\varepsilon_{F,f} = \frac{w_{U-i}}{L_{W,V-i}} \rightarrow L_{W,V-i} = \frac{w_{U-i}}{\varepsilon_{F,f}} \tag{12}$$

where $\varepsilon_{F,f}$ = failure strain of filaments. The set of pair of values ($L_{W,V-i}$; M_{U-i}) resulting from the recursive computation according to Eq. (10) represents the distribution of the filaments' deformation lengths inside the multifilament yarn bridging a single crack. To enable a graphic representation analogous to Fig. 8 (right) the distribution-curve based on discrete pair of values ($L_{W,V-i}$; M_{U-i}) is transformed via linear interpolation to a quasi-continuous distribution curve based on pairs of values ($L_{W,V-i}$; n_j), where n = individual filament number. The processing of this interpolation is depicted in Fig. 14.

A calculated total number of filaments N_{calc} results from the numerical processing as described above. In the specimen the number of inactive filaments N_P can be determined by counting the filaments, which are pulled-out completely. Comparing $N_{calc} + N_P$ and the physical number of filaments in the yarn N, three cases must be distinguished:

a) $N_{calc} + N_p < N$: An iterative recalculation of $L_W(n)$ is performed with the stepwise reduced failure strain of filaments $\varepsilon_{F,f}$ until the condition $N_{calc} + N_p = N$ is satisfied. This case indicates a loss of filament strength, according to the reduction of $\varepsilon_{F,f}$.
b) $N_{calc} + N_p = N$: The calculation can be completed.
c) $N_{calc} + N_p > N$: The condition $N_{calc} + N_p = N$ cannot be satisfied. This case indicates a cross-link breakdown instead of filament failure. The number of excessive filaments $N - (N_{calc} + N_p)$ and their deformation lengths indicate to what extent the breakdown of cross-links occurs [14].

5. Application of calculation model on experimental results

The method of recursive calculation of distribution of deformation lengths (cf. Section 3.4) was used to conclude from experimental results (cf. Section 2.3) as to the bonding situation inside the multifilament yarn. A distribution curve of deformation lengths $L_W(n)$ was computed for each simplified pullout-crack width curve as pictured in Figs. 2 and 3. In addition to the $L_W(n)$-curves, filament strengths β_F are indicated, which were used to calculate the curves displayed. The filament strength has to be defined at the beginning of calculation process.

In Fig. 15 the results of the numerical processing of pullout data of matrix M1 specimens are shown. During ageing a decrease in the deformation lengths of almost all filaments can be reported. The minimum deformation length $L_{W,min}$ at filament number $n = 4800$ is reduced from 7 mm (reference curve) to 0.7 mm (360 d ageing). These reductions happen mainly in the sleeve filaments. The sleeve filaments have relatively short deformation lengths and are therefore arranged in the upper part of y-axis in Fig. 15 (see also Section 4.2). Only the deformation lengths of core filaments ($n = 1$ ⋯ approximately 200) show nearly no change with increasing age. The core filaments possess the largest deformation lengths (see Section 4.2, in this case: $L_W > 50$ mm). At all specimen ages higher numbers of

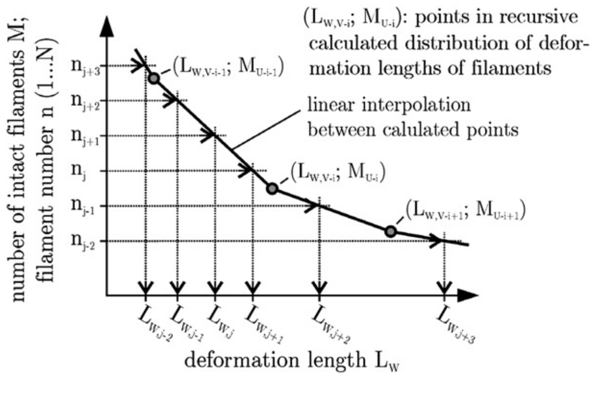

Fig. 14. Determination of a quasi-continuous distribution-curve by means of linear interpolation between discrete points ($L_{W,V-i}$; M_{U-i}) resulting from recursive calculation process according to Fig. 10.

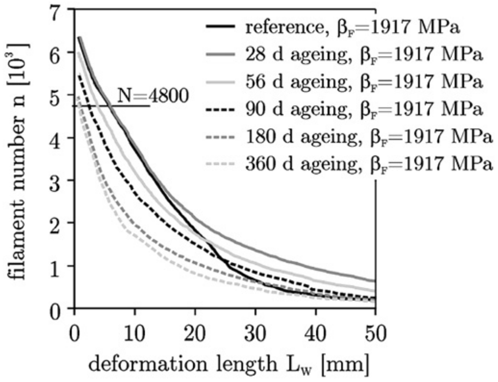

Fig. 15. Calculated distribution of filament deformation lengths for matrix M1 specimens (based on Fig. 2).

filaments $N_{calc}+N_p$ were determined than were physically present in the specimen (three multifilament yarns → $N=4800$). All calculations were performed with an initial filament strength of $\beta_F=1917$ MPa.

Fig. 16 displays the results for specimens made of matrix M2. Here the decrease of the individual deformation lengths of the filaments is more pronounced than in Fig. 15. The minimal deformation length $L_{W,min}$ at filament number $n=4800$ is reduced from 7.5 mm (reference curve) to 2 mm (56 d ageing). From this state of ageing until an age of 360 days, the filament strength used in calculation was reduced from 1917 MPa to 1451 MPa to satisfy the condition $N_{calc}+N_p=N=4800$. This indicates a reduction of filament strength with increasing age. At matrix M1 no such strength reduction in the calculation process was necessary due to its less pH-value and therefore reduced alkaline attack to the glass filaments. Only in reference specimens and after 28 days accelerated ageing higher numbers of filaments $N_{calc}+N_p$ were determined than were physically present in the yarn ($N=4800$).

6. Discussion of results

At this point the results of mechanical testing (cf. Section 3.4), of numerical modelling (cf. Chapter 4), and of micro-structural investigation (cf. Section 2.4) can be discussed with a view to identify the mechanisms which lead to the degradation in crack-bridging behaviour of multifilament yarn during ageing.

The reference specimens made of matrices M1 and M2 show favourable pullout behaviour. The higher pullout force of the matrix M2 specimens in comparison to the reference specimens made of matrix M1 (cf. Figs. 3 and 5) is attributed to the higher Portland cement clinker content in matrix M2. It leads to a faster hydration process and with it to a more homogeneous structure of the C–S–H phases after reference storage. The well developed bond between filaments and matrices of both M1 and M2 enables the slip of filaments relative to the matrix at high filament stress levels instead of filament failure and with that a high pullout work. This is substantiated by the distribution of deformation lengths, which indicates a significant potential for cross-link breakdown of reference specimens (cf. Figs. 15 and 16). This is indicated by a calculated filament number $n>4800$.

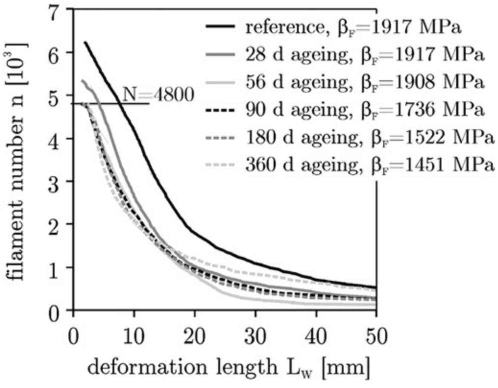

Fig. 16. Calculated distribution of filament deformation lengths for matrix M2 specimens (based on Fig. 3).

The mechanical performance of both specimen types decreases differently to one another when accelerated ageing is applied. In the case of matrix M1 the degradation is less pronounced than in the specimens made of matrix M2. This is due to the hydration characteristics of CEM III cement, causing a low production of C-H which is furthermore consumed continuously by the pozzolana (fly ash and silica fume) in the formation of C–S–H phases. As a result the morphology of the matrix-fibre interface is dominated by delicate hydration products (cf. Fig. 8). These slender filament wrappings become increasingly denser with increasing age, as substantiated by decreasing deformation lengths of filaments (cf. Fig. 15). The densification in the interface between matrix and filaments during ageing leads to the decrease of the maximum fibre pullout force and pullout work already described (cf. Figs. 3 and 4). However, up to 360 days of accelerated ageing, the filament–matrix interface still allows the de-bonding and slip of filaments if the filaments are highly strained in the vicinity of a matrix crack, as evidenced by the remaining potential for cross-link breakdown (cf. Fig. 15).

The specimens made of matrix M2 show a more pronounced degradation of mechanical performance with age. The volume of C-H produced in the hydration process is higher than in matrix M1. Hence, on the one hand a higher C-H content remains in the microstructure. On the other hand the C–S–H phases formed during the pozzolanic reaction feature a different morphology, characterized by a very dense structure (cf. Fig. 9). Around the filament surfaces both hydration products initially form thin-walled, slender wrappings, which become increasingly compact and stiffer, producing inflexible crusts. The rapid densification process in the matrix-filament interface with increasing age is substantiated by rapidly decreasing deformation lengths (Fig. 16). Thus, failure strain of the filaments is reached at smaller crack widths. Also the crusts restrict the slip of filaments in the vicinity of a matrix crack (no potential for cross-link breakdown, Fig. 16).

Furthermore, these brittle crusts can flake off locally if the covered filament is strained. This can happen because of pronounced differences in strain capacity between filament (high) and covering crust (low). At the points where the cross-section changes from a “composite-type”, consisting of filament and enveloping crust, to the original filament, high stress concentrations can arise due to the notch effect, which leads to the premature failure of the filament. This phenomenon was simulated at an isolated filament using a micro manipulator installed inside the electron microscope. In Fig. 17 the filament is shown after acting to the filaments crusts made of C–H and C–S–H phases by means of manipulator's needle tip. The crusts partially flaked off. An abrupt change in the cross section is clearly visible.

This effect is represented by reduced strength of filaments β_F (cf. Fig. 16). Also, local notching of filament surface due to the less than critical growth of surface flaws [7,8] cannot excluded. These multiple effects explain the decrease in performance of aged matrix M2 specimens in comparison to the matrix M1 based specimens.

7. Conclusions

Degradations in mechanical performance of crack-bridging multifilament yarns can in the main be traced back to changes in the microstructure in the interface between matrix and filaments and between the filaments themselves, respectively. In addition to microstructural investigations of interface morphology, this could be evidenced by means of modelling the time-dependent changes in

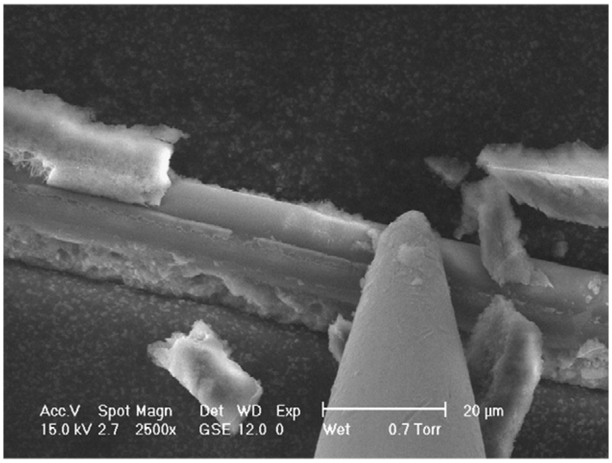

Fig. 17. Removal of brittle crusts consisting of C–S–H phases and CH phases using a micro manipulator inside the ESEM.

distribution of filament deformation lengths $L_W(n)$. This distribution $L_W(n)$ can be computed from experimental pullout data according to a simple phenomenological model. With applicable identification of $L_W(n)$, densifications in the filament–matrix interface can be concluded, which reduce the deformability of filaments, hence causing a precipitate filament failure. Furthermore, the changes in the morphology can lead to the decrease in filament strength. The causes of losses in filament strength can be both mechanical notching due to the scaling of mineral incrustations from the filament surface as well as the chemical notching of the filaments' bulk glass, referred to as the less than critical growth of surface flaws. Beside this the potential for cross-link breakdown can be estimated by mean of the new model. It is an important composite feature to assure ductile crack-bridging through multifilament yarns at high load level.

Acknowledgements

The results were obtained in a project initiated in the Collaborative Research Centre SFB 528 "Textile Reinforcement for Structural Strengthening and Retrofitting" financed by the German Research Foundation "DFG". The authors would like to acknowledge with gratitude the foundation's financial support.

References

[1] W. Brameshuber (Ed.), Textile Reinforced Concrete, RILEM Report 36, State-of-the-Art Report of RILEM Technical Committee 201-TRC, RILEM Publications S.A.R.L., 2006.
[2] A. Paul, Chemical durability of glasses; a thermodynamic approach, J. Mater. Sci. 12 (11) (1977) 2246–2268.
[3] V. Yilmaz, F. Glasser, Reaction of alkali-resistant glass fibres with cement. Part 2: durability in cement matrices conditioned with silica fume, Glass Technol. 32 (4) (1991) 138–147.
[4] S. Hempel, M. Butler, Microscopic investigations on durability of textile reinforced concrete, Proc 11th Euroseminar on microscopy applied to building materials, Porto, 2007.
[5] M. Tomozawa, Fracture of glasses, Annu. Rev. Mater. Sci. 26 (1996) 43–74.
[6] T.A. Michalske, S.W. Freiman, A molecular mechanism for stress corrosion in vitreous silica, J. Am. Ceram. Soc. 66 (4) (1983) 284–288.
[7] P. Purnell, N.R. Short, C.L. Page, A static fatigue model for the durability of glass fibre reinforced cement, J. Mater. Sci. 36 (22) (2001) 5385–5390.
[8] J. Orlowsky, M. Raupach, Durability model for AR-glass fibres in textile reinforced concrete, Mat. Struct. 41 (7) (2008) 1225–1233.
[9] P.J.M. Bartos, W. Zhu, Effect of microsilica and acrylic polymer treatment on the ageing of GRC, Cem. Concr. Compos. 18 (1) (1996) 31–39.
[10] A. Bentur, Role of interfaces in controlling durability of fiber-reinforced cements, J. Mater. Civil Eng. 12 (1) (2000) 2–7.
[11] W. Zhu, P.J.M. Bartos, Assessment of interfacial microstructure and bond properties in aged GRC using a novel microindentation method, Cem. Concr. Res. 27 (11) (1997) 1701–1711.
[12] M.A. Glinicki, A.M. Brandt, Quantification of glass fibre–cement interfacial properties by SEM-based push-out test, Proc 5th int RILEM workshop high performance fiber reinforced cement composites, Proc 53 RILEM, 2007, pp. 343–355.
[13] H. Schorn, Ein Verbundmodell für Glasfaserbewehrungen im Beton, Bautechnik 80 (3) (2003) 174–180.
[14] M. Butler, Zur Dauerhaftigkeit von Verbundwerkstoffen aus zementgebundenen Matrices und alkaliresistenten Glasfaser-Multifilamentgarnen, Dissertation at the Institute of Construction Materials, TU Dresden (2009) (in German).
[15] M. Butler, V. Mechtcherine, S. Hempel, Experimental investigations on the durability of fibre–matrix interfaces in textile-reinforced concrete, Cem. Concr. Compos. 31 (2009) 221–231.
[16] M. Butler, V. Mechtcherine, S. Hempel, Durability of textile reinforced concrete made with AR glass fibre: effect of the matrix composition, Mat. Struct. 43 (2010) 1351–1368.